ADVANCED FUNCTIONAL MATERIALS

www.afm-journal.de

Interface Engineering for Both Cathode and Anode Enables Low-Cost Highly Efficient Solution-Processed CdTe Nanocrystal Solar Cells

Zhitao Rong, Xiuzhen Guo, Shaoshan Lian, Songwei Liu, Donghuan Qin, Yueqi Mo,* Wei Xu, Hongbin Wu, Hong Zhao, and Lintao Hou**

Low-cost solution-processed CdTe nanocrystal (NC) solar cells always suffer from a high interface energy barrier and unbalanced hole/electron transport as well as anisotropic atom diffusion on the CdTe surface due to the limited amount of hole/electron interface materials or the difficulty in interface processing. In this work, a novel strategy is first adopted with gradient electron transport layer (CdS/CdSe) modification in the cathode and a new crosslinkable hole transport polymer (P-TPA) implantation in the anode. The carrier recombination at interfaces is greatly decreased and thus the carrier collection is increased. Moreover, the light harvesting is improved both in short and long wavelength regions, making J_{sc} and V_{oc} increase simultaneously. A champion solar cell shows a very high power conversion efficiency of 9.2% and an outstanding J_{sc} of 25.31 mA cm^{-2}, which are among the highest values for all solution-processed CdTe NC solar cells with a superstrate structure, and the latter value is even higher than that of traditional thick CdTe thin-film solar cells (2 µm) via the high temperature close space sublimation method. This work demonstrates that facile surface modifications in both the cathode and anode with stepped extraction and organic–inorganic hybridization are very promising in constructing next-generation highly efficient NC photovoltaic devices.

1. Introduction

Solution-processed CdTe nanocrystal (NC) solar cells have attracted much attention in recent years because they can be manufactured via solution processing with the feasibility using low-cost roll-to-roll large-area printing techniques under ambient fabricating conditions.[1–7] The performance of CdTe NC solar cells has been improved rapidly for power conversion efficiency (PCE) from ≈3%[8] to 8.54%[9] through optimization of NC sintering[10,11] and n-type acceptor[12–14] as well as device architecture.[15,16] It is noted that the highest PCE of 12.3% is obtained to date for CdTe NC solar cells with a device structure of ITO/CdTe/In: ZnO/metal; however, as there exists a work function mismatch between CdTe (≈5.2 eV) (Figure S1, Supporting Information) and ITO (≈4.7 eV),[17] a voltage/light soaking process must be undertaken before *J*–*V* measurement.[1] Even worse, the device efficiency decays rapidly about 30% after several days due to the recovery of work function mismatch existed in the ITO/CdTe interface.[9]

For solving this problem, the incorporation of a favorable electron transport layer (ETL) in the cathode is proposed. For example, a thin ZnO layer is inserted between ITO and CdTe; however, low-quality CdTe NC thin film is formed on top of the ZnO film due to large lattice mismatch, leading to the device performance instability.[18,19] Unlike ZnO or other n-type interface materials such as TiO_2,[20] CdS has a low lattice mismatch for CdTe, so high-quality CdTe active layer can be well developed.[21–23] However, since CdS has a strong parasitic absorption in the 300–525 nm range, a low spectrum response is produced in short wavelengths, resulting in a low J_{sc}.[24,25] In order to improve the J_{sc}, decreasing the thickness of the CdS layer has been adopted in close space sublimation (CSS)-processed CdTe thin-film solar cells, while too thin CdS layer would reduce effective electron extraction.[26,27] Since Se atom has higher solubility in CdTe due to its similar size to Te atom than S atom and the formed $CdSe_xTe_{1-x}$ layer is photoactive during the annealing process, CdSe has been used to replace CdS as n-type partner in CdTe NC solar cells.[28–30] Thus the parasitic absorption in CdSe is decreased, which is beneficial to improve the device performance. Furthermore, due to the bandgap bowing effect, the formed $CdSe_xTe_{1-x}$ alloy shows a narrower bandgap than pure CdTe, which means that photon absorption can be extended to longer wavelengths. It is reported

---

Z. Rong, X. Guo, S. Lian, S. Liu, Prof. D. Qin, Prof. Y. Mo, Prof. W. Xu, Prof. H. Wu
Institute of Polymer Optoelectronic Materials & Devices
State Key Laboratory of Luminescent Materials & Devices
South China University of Technology
Guangzhou 510640, China
E-mail: qindh@scut.edu.cn; pomoy@scut.edu.cn

H. Zhao, Prof. L. Hou
Guangdong Provincial Key Laboratory of Optical Fiber Sensing and Communications
Guangzhou Key Laboratory of Vacuum Coating Technologies and New Energy Materials
Siyuan Laboratory
Department of Physics
Jinan University
Guangzhou 510632, China
E-mail: thlt@jnu.edu.cn

The ORCID identification number(s) for the author(s) of this article can be found under https://doi.org/10.1002/adfm.201904018.

DOI: 10.1002/adfm.201904018

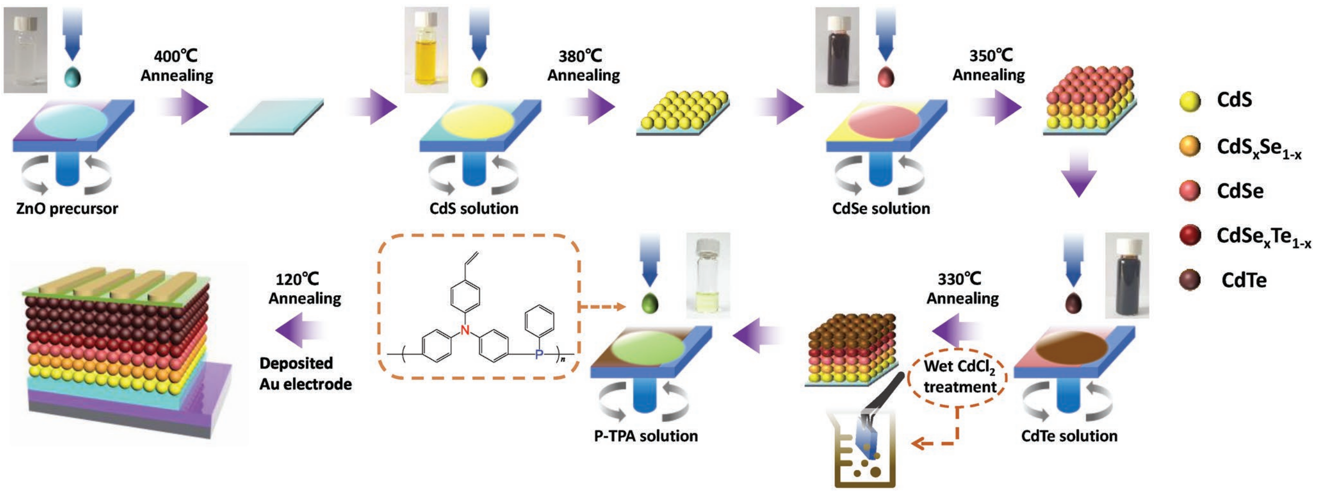

Figure 1. A schematic outline of the layer-by-layer process for making CdTe NC solar cells.

that the energy bandgap as low as 1.32 eV is obtained with $x \approx 0.38$ for $CdSe_xTe_{1-x}$, which is much smaller than 1.5 eV for CdTe.[31,32] However, devices with a single CdSe ETL may suffer from low V_{oc} and fill factor (FF) due to the large electron injection barrier and interface defects in $ZnO/CdSe_xTe_{1-x}$, which has been confirmed in the CSS-processed CdTe solar cells with the SnO_2/CdSe structure.[33] Thus, new cathode interface strategy should be developed for solution-processed CdTe NC solar cells. On the other hand, anode modification is also very important for increasing V_{oc} of NC solar cells. For example, Cu doping has been widely adopted to increase V_{oc} for most high-efficiency CdTe thin film solar cells prepared by CSS method.[34] However, excessive Cu diffusion will deteriorate the electronic properties of the n-type layers, resulting in the drastic degradation of the device performance.[35,36] Furthermore, since there exist a lot of crystal boundaries in the solution-processed CdTe layer, it is very difficult to control the Cu doping concentration, leading to the worse repeatability of device performance. Therefore, it is suggested that introducing an organic hole transport layer (HTL) before the deposition of Au contact electrode is very effective for increasing V_{oc}. By introducing a polymer poly(diphenylsilane-*co*-4-vinyl-triphenylamine) layer as HTL between the CdTe NC film and the Au electrode, the carriers become more balanced and the interface recombination is decreased, making V_{oc} increased from 0.59 to 0.66 V.[37] Thus, it can be seen that interface engineering for both cathode and anode is extraordinarily necessary for further developing highly efficient CdTe NC solar cells in this field.

In this work, we demonstrate multilayer electron acceptors of ZnO/CdS/CdSe and a novel new crosslinkable polymer poly(phenylphosphine-*co*-4-vinyl-triphenylamine) (P-TPA) to simultaneously increase V_{oc} and J_{sc} as well as PCE of low-cost solution-processed CdTe NC solar cells with a superstrate structure of ITO/ZnO/CdS/CdSe/CdTe/P-TPA/Au. The presence of a ZnO layer can decrease the interface recombination in CdS/ITO or CdSe/ ITO and thus the parallel resistance is increased.[19] The incorporation of *n*-type CdS/CdSe NC and *p*-type P-TPA endows CdTe NC solar cells with a high V_{oc} with less interface defects. The formed $CdSe_xTe_{1-x}$ alloy with very strong photon-active property improves J_{sc} of the CdTe NC cells with an abroad spectrum response in entire wavelength region. As the highest-energy occupied molecular orbital (HOMO) level of P-TPA matches well with the work function of CdTe NC, hole carrier extraction from the CdTe layer becomes more efficient than the device without P-TPA. In the end, a very high device performance is obtained by introducing the above interfacial modification strategy with the V_{oc}, J_{sc}, and PCE of 0.72 V, 25.31 mA cm^{-2}, and 9.20%, respectively. To the best of our knowledge, the PCE and J_{sc} achieved are the highest values ever reported for low-cost solution-processed CdTe NC superstrate solar cells. This work not only sheds light on the internal reasons behind performance improvements, but also demonstrates that simultaneous cathode/anode interface regulation is very promising in the future CdTe NC solar cell manufacturing.

2. Results and Discussion

The CdTe NC solar cells with a superstrate structure of ITO/ZnO/CdS/CdSe/CdTe/P-TPA/Au (**Figure 1**) are fabricated via a layer-by-layer spin-coating and sintering process. The ZnO thin film prepared by decomposition of the Zn^{2+} carboxyl precursor is used as the ETL. Since the one-layer CdS NC is essential to decrease the misfit dislocations caused by the large lattice mismatch between ZnO and CdTe, low dangling bonds densities at interfaces can be obtained with the insertion of CdS layer.[38,39] In other words, the one-layer CdS layer with a stepwise change of lattice constant allows a considerable reduction of misfit dislocations, resulting in an electrical passivation. The two-layer CdSe plays a similar role in further decreasing the lattice mismatch, and at the same time it acts as the acceptor. For simplicity, the CdS and CdSe layers are called gradient electron transport layers due to the matched energy level alignment. The six-layer CdTe NC is used as the donor. A new crosslinkable polymer, P-TPA (Figure 1), with a high HOMO level (>5.5 eV) is spin-cast onto the CdTe layer. Due to the high electron affinity and high resistance of CdTe NC film, P-TPA can be used as HTL to reduce interfacial charge recombination.

The crosslinkable polymer P-TPA has many merits for CdTe NC solar cells: 1) P atoms from group V on the polymer

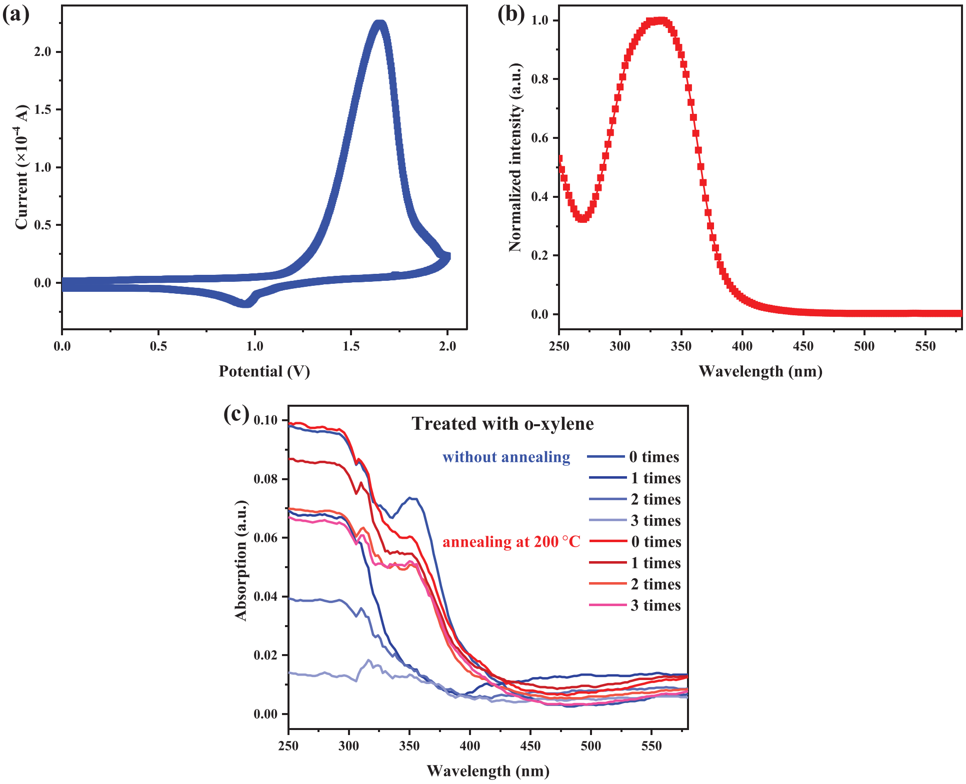

Figure 2. a) Cyclic voltammetry curve of P-TPA in acetonitrile solution. b) UV–vis spectrum of P-TPA in chloroform solution. c) Absorption spectra of P-TPA layer w/o o-xylene treatment.

backbone can bond tightly to Cd compared to Si atoms from group IV on the polymer backbone of Si-TPA; 2) good band alignment between P-TPA and CdTe leads to an improved hole collection efficiency; 3) the dipole layer formed between P-TPA and CdTe facilitates hole injection from CdTe NC to Au; 4) better adhesion of P-TPA onto the CdTe surface by crosslinking and P—Cd bonds, compared to Si-TPA; 5) the P-doped CdTe in the interface is expected to increase the V_{oc} of the CdTe NC solar cells, which is confirmed by Burst et al. recently for CSS-processed CdTe solar cells with V_{oc} breaking 1 V.[21]

To study the energy level property of P-TPA, electrochemical measurement is conducted. The cyclic voltammetry result is shown in **Figure 2**a. The electrochemical property of P-TPA shows oxidation potential (E_{ox}) at 1.33 V, which is used to estimate a HOMO energy level of −5.73 eV, according to the empirical formulas $E_{HOMO} = -(E_{ox} + 4.4)$ (eV).[40] The absorption edge for P-TPA in chloroform is 381 nm (Figure 2b); therefore, the bandgap of P-TPA is 3.26 eV and the corresponding lowest unoccupied molecular orbital (LUMO) level is −2.47 eV. For investigating the chemical resistance of this new-type crosslinkable material to o-xylene, the absorption spectra are measured via UV–vis spectroscopy (Figure 2c). The data show that the crosslinkable P-TPA polymer is almost completely resistant to o-xylene, indicating it is a promising HTL with the feasibility to be used in a multilayer device structure with a solution process.

For probing the strong interdiffusion of CdTe with CdSe and the poor solubility of CdTe with CdS, focused ion beam (FIB) cross sections across ITO/ZnO/CdS/CdSe/CdTe/P-TPA/Au device are prepared for analysis with the bright-field (BF) transmission electron microscope (TEM) and high resolution transmission electron microscope (HRTEM) images (**Figure 3**). BF-TEM image is acquired by transmitted electrons, which is mass- and crystallinity-dependent with high mass and crystallinity appearing dark for inorganic nanocrystals in bright field image. It can be seen that the thickness of ZnO is ≈40 nm and the thickness of CdS/CdSe/CdTe/P-TPA is ≈700 nm, which is in accordance with the number of spin-coatings. The measured CdS NC lattice parameter is 3.359 Å, which corresponds to the (111) lattice plane of the zinc-blende CdS structure. In the CdS/CdSe interface, the measured lattice parameter is d = 3.407 Å, which is between 3.359 Å for the (111) lattice parameter of zinc-blended CdS and 3.51 Å for the (111) lattice parameter of zinc-blende CdSe. Therefore, it can be concluded that a very thin homogeneous CdS_xSe_{1-x} alloy is formed in the CdS/CdSe interface, which is beneficial for electron transport due to the graded levels of energy and the decreased defects between CdS and CdSe. For CdSe and CdTe NC active layers, there are no obvious boundaries in the entire two different thin films. The measured lattice parameter for the $CdSe_xTe_{1-x}$ grain is d = 3.89 Å, which is consistent with the value in previous literatures.[41,42] The whole CdTe and CdSe active layers combine into a homogeneous $CdSe_xTe_{1-x}$ alloy film, which is very important to improve the lifetime of photogenerated carriers and device performance. As the thickness of the CdSe NC layer is only 80 nm, the CdSe thin layer should be fully doped with Te into the formation of the $CdSe_xTe_{1-x}$ alloy.

In order to quantitatively detect the distribution of elements, the cross-sectional compositional variations of the

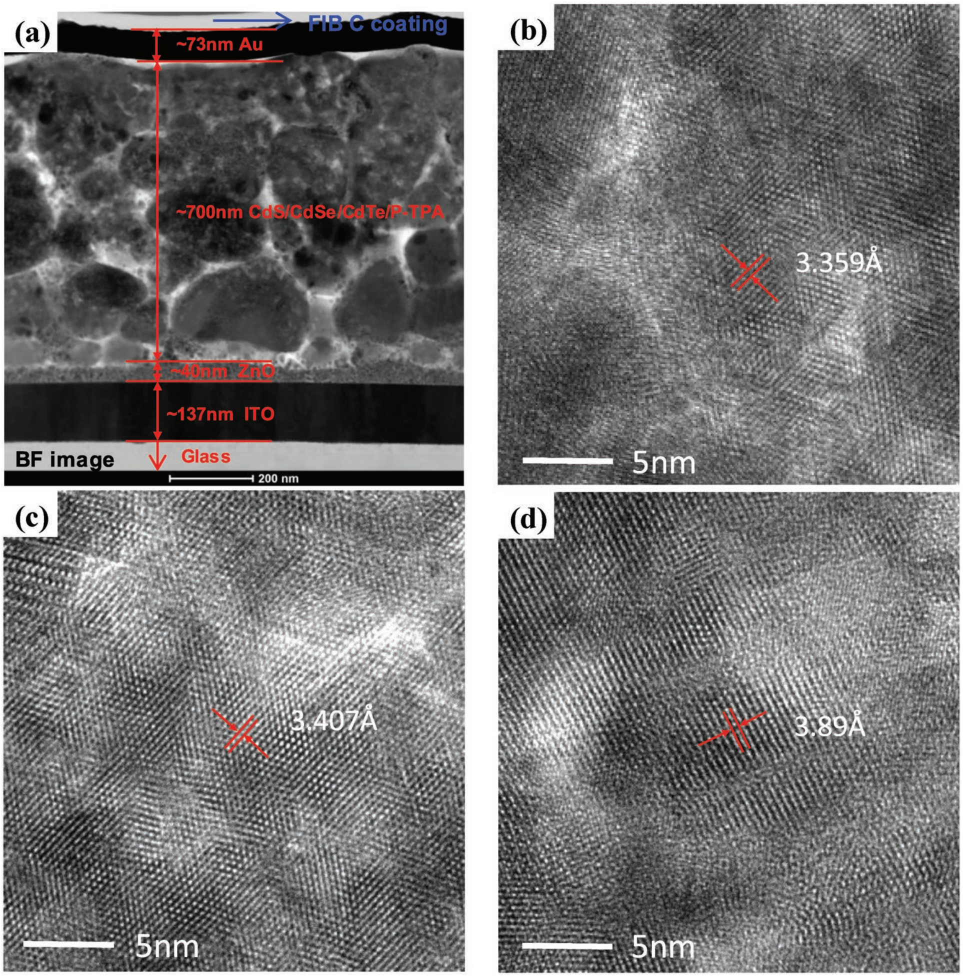

Figure 3. a) A BF cross-sectional TEM image of CdTe NC solar cells (device structure: ITO/ZnO/CdS/CdSe/CdTe/P-TPA/Au); b) HRTEM image of the CdS layer; c) HRTEM image of homogeneous CdS_xSe_{1-x} alloy formed in the CdS/CdSe interface; d) HRTEM image of homogeneous $CdSe_xTe_{1-x}$ alloy.

whole device marked with different colors are characterized by energy-dispersive spectrometry (EDS) with the reference to high-angle annular dark-field scanning transmission electron microscope (HAADF-STEM) (**Figure 4**). The normalized atomic percentage of S, Se, Te, and Cd in CdTe NC solar cells by using EDS line scan is also presented in Figure S2 (Supporting Information). HAADF-STEM image is produced by highly scattered electrons, which intensity is dependent on mass with heavy atoms observed brighter and light atoms difficultly observed. It is found that the Zn and S elements are fixed near the ITO substrate, implying that the diffusion of Zn and S into the CdSe or CdTe layer is very low. On the contrary, Se and Te elements are distributed in the whole CdSe and CdTe regions, corresponding to the high diffusion of Se and Te into each other. The results demonstrate that the thin CdSe NC layer can be consumed entirely during the annealing process. Due to the bandgap bowing effects,[43,44] the formed $CdSe_xTe_{1-x}$ alloy presents bandgap grading property, which should extend the spectrum response of CdTe NC solar cells. Thus it can be speculated that the device performance can be further improved with the adoption of both the CdS/CdSe gradient ETLs and P-TPA HTL.

The effect of CdS and CdSe NC thicknesses on the absorption of ITO/ZnO/CdS/CdSe film is shown in Figure S3a,b (Supporting Information). It is found that the absorption of ITO/ZnO/CdS layer increases almost linearly with the CdS thickness from 0 to 125 nm. Similar results are found for ITO/ZnO/CdS(25 nm)/CdSe samples with different thicknesses of CdSe. The results indicate that the thickness of CdS or CdSe layer plays a significant role in determining the performance of CdTe NC solar cells. In order to investigate the effect of the CdS/CdSe gradient ETLs thickness on the device performance, the devices with a simple ITO/ZnO/CdS/CdSe/CdTe/Au structure are fabricated with the current density–voltage (J–V) curves exhibited in Figure S4 (Supporting Information) and the photovoltaic data summarized in Table S1 (Supporting Information). When the CdSe NC layer is fixed at ≈80 nm (2 layers), the device performance increases first and then decreases linearly with the increase CdS NC layer thickness, indicating the thickness of CdS NC film has a big effect on J_{sc}. It can be concluded that a very thin CdS layer from 0 to 25 nm is attributed to reduce carriers recombination at the interface of ZnO/CdSe,[33] leading to improvement in device performance. However, as the parasitic absorption of CdS layer increases

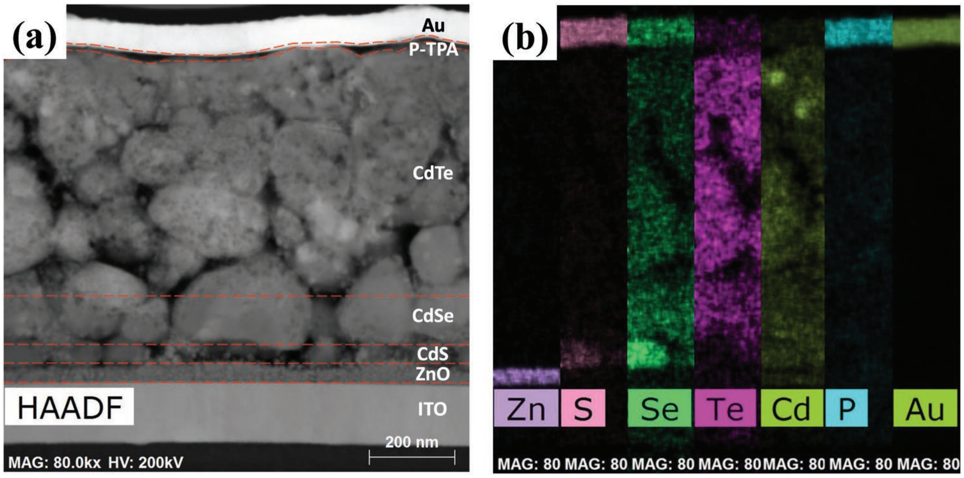

Figure 4. a) A cross-sectional HAADF-STEM image of CdTe NC solar cells. b) The distribution of Zn, S, Se, Te, Cd, P, and Au elements in the device as characterized by EDS.

with increasing its thickness,[23] the thick CdS layer from 25 to 100 nm can greatly reduce the spectrum response in short wavelengths, leading to a low J_{sc}. As we know, graded CdS_xSe_{1-x} and $CdSe_xTe_{1-x}$ can be formed easily in the case of CdTe NC solar cells with the device configuration of ITO/ZnO/CdS/CdSe/CdTe/Au (Figure 4). High device performance is expected when changing the CdSe thickness from 40 to 160 nm. In case of the optimized CdS thickness of 25 nm, the device performance increases with increasing the CdSe NC film thickness from 40 to 80 nm, then decreases linearly when the thickness of the CdSe NC film is further increased. Therefore, the optimized thicknesses of CdS and CdSe NCs are 25 and 80 nm, respectively. Since CdS_xSe_{1-x} is photon-inactive and $CdSe_xTe_{1-x}$ is photon-active as well as a small amount of Te atoms diffuse into the CdS layer (Figure 4), the effect of CdTe thickness variation on device performance is not easily clarified. However, it is sure that all factors, such as interface recombination, parasitic absorption and electron transport that influence device performance can obtain the best synergy in case of 25 nm CdS and 80 nm CdSe in the CdTe NC device. To exhibit the advantages of the P-TPA, CdTe NC solar cell with a superstrate structure of ITO/ZnO/CdS/CdSe/CdTe/P-TPA/Au is also constructed. The optimized thickness for P-TPA is 15 nm at 120 °C (Figure S5a and Table S2, Supporting Information). Further increase or decrease of the P-TPA thickness may deteriorate device performance due to the increase of contact resistance from a thick HTL or insufficient coverage of the CdTe NC thin film by a thin HTL. The optimized crosslinking temperature of P-TPA is 120 °C (Figure S5b and Table S2, Supporting Information), which is related to the best hole mobility at this temperature compared to other crosslinking temperatures (Figure S6, Supporting Information).

Figure 5a shows the *J–V* curves of four kinds of CdTe NC solar cells under optimized conditions with the performance parameters such as V_{oc}, J_{sc}, FF, and PCE summarized in **Table 1**. The NC solar cell with only a single CdS NC ETL (Device A: ITO/ZnO/CdS/CdTe/Au) shows a V_{oc} of 0.62 V, a J_{sc} of 18.83 mA cm^{-2}, and a FF of 47.68%, resulting in a PCE of 5.60%. For the CdSe NC as the ETL, the CdTe NC solar cell (Device B: ITO/ZnO/CdSe/CdTe/Au) shows a V_{oc} of 0.58 V, a J_{sc} of 18.76 mA cm^{-2}, and a FF of 53.6%, leading to a PCE of 5.86%. Compared with above standard CdS and CdSe solar cells, the CdS/CdSe gradient ETLs solar cell (Device C: ITO/ZnO/CdS/CdSe/CdTe/Au) shows simultaneous improvement in V_{oc}, J_{sc}, and PCE with values of 0.65 V, 23.18 mA cm^{-2} and 7.82%. We emphasize that the high J_{sc} obtained is among the

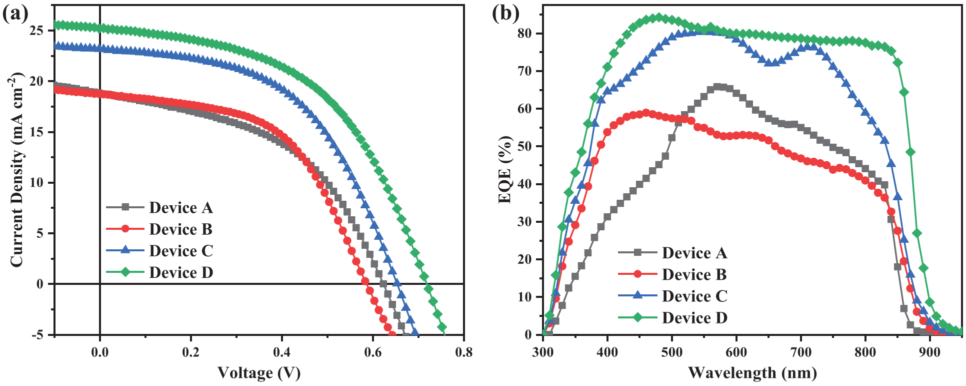

Figure 5. a) *J–V* curves of four kinds of CdTe NC solar cells under 100 mW cm^{-2} (AM 1.5G) illumination and b) corresponding EQE spectra.

Table 1. The performance parameters of low-cost solution-processed CdTe NC solar cells with different device architecture.

Device architecture	V_{oc} [V]	J_{sc} [mA cm^{-2}]	FF [%]	PCE [%]	R_s [Ω cm^2]	R_{sh} [Ω cm^2]
ITO/ZnO/CdS/CdTe/Au	0.62	18.83	47.68	5.60	9.89	117.37
ITO/ZnO/CdSe/CdTe/Au	0.58	18.76	53.6	5.86	10.4	360.3
ITO/ZnO/CdS/CdSe/CdTe/Au	0.65	23.18	52.37	7.82	8.38	424.27
ITO/ZnO/CdS/CdSe/CdTe/P-TPA/Au	0.72	25.31	50.49	9.20	8.06	263.50

highest values ever reported for solution-processed CdTe NC solar cells with a superstrate structure due to the suppressed defects in the ZnO/CdSe interface, demonstrating that the combined CdS/CdSe gradient ETLs facilitate charge extraction and collection. Furthermore, the thin CdS NC layer in Device C can effectively improve the V_{oc}, leading to the PCE value 40% and 33% higher than that of the Device A and Device B, respectively. For the best CdTe NC solar cell with optimized anode/cathode interfaces (Device D: ITO/ZnO/CdS/CdSe/CdTe/P-TPA/Au), the V_{oc} and J_{sc} are 0.72 V and 25.31 mA cm^{-2}, respectively, delivering an excellent high PCE of 9.20%. This PCE value is increased by 18% compared to Device C without P-TPA interface modification. It can be found that the improvement of efficiency in CdTe NC solar cells with a P-TPA HTL comes mainly from the increase in V_{oc} from 0.65 to 0.72 V and J_{sc} from 23.18 to 25.31 mA cm^{-2}. To the best of our knowledge, the PCE obtained here is the highest PCE value ever reported for solution-processed CdTe NC solar cells with a superstrate structure. Moreover, the dark *J–V* curves of the four kinds of devices are presented in Figure S7 (Supporting Information). It is clearly seen that the dark current density of the Device D is significantly suppressed compared to other three control devices, which is also beneficial to improve V_{oc}.

Figure 5b shows the external quantum efficiency (EQE) spectra of corresponding devices. The decreased EQE value in the short wavelength region for the CdS-based CdTe NC Device A suggests that the CdS NC layer is photoinactive, and the light absorbed by the CdS layer can not generate photocurrent, which is consistent with a previous report.[24] For the gradient ETLs Device C, the EQE spectrum shows obvious high value in both short and long wavelength regions as a result of the formation of low-bandgap $CdSe_xTe_{1-x}$ alloy and the reduction of interface defects. The EQE spectrum of the Device D with P-TPA HTL shows a nearly rectangular shape with average photon-to-carrier efficiency of 80%, indicating nearly zero loss in the wavelength region from 400 to 850 nm. When the EQE curves are integrated, the calculated J_{sc} of 25.28 mA cm^{-2} is predicted, which is well consistent with the measured J_{sc} presented in the *J–V* curve. We emphasize that the J_{sc} obtained here is among the highest values for all solution-processed CdTe NC solar cells, and even higher than that of CdTe thin-film solar cells prepared by a CSS method with CdTe thickness up to 2 µm.[45]

To gain more insight into the effect of gradient ETLs and P-TPA HTL on the CdTe NC solar cell performance, capacitance–voltage (*C–V*) analysis is carried out by increasing bias voltage at a constant frequency of 1000 Hz to investigate the built-in electric field of the NC solar cells.[16,46,47] As shown in **Figure 6**a, *C–V* curves are plotted based on the Mott–Schottky equation[48]

$$C^{-2} = \frac{2}{A^2 q \varepsilon_0 \varepsilon N_A}(V_{bi} - V) \tag{1}$$

where the parameters A, ε, ε_0, V_{bi}, and N_A are the device active area, relative dielectric constant (10.6), vacuum permittivity, built-in potential, and net acceptor concentration, respectively. The V_{bi} can be extracted at a forward bias from the extrapolated intersection of the slope and x axis. The V_{bi} of the Device C (CdS/CdSe gradient ETLs) is 0.65 V, which is higher than 0.62 V for the Device A and 0.55 V for the Device B. The V_{bi} of the Device D is 0.73 V, which is much higher than the Device C without P-TPA HTL. The V_{bi} values agree well with the V_{oc} values from the *J–V* curves. To further examine the effect of P-TPA HTL on the carrier recombination of NC solar cells, the charge recombination lifetime is investigated by transient photovoltage (TPV). The charge recombination processes are studied by tracking the transient open-circuit voltage related to charge population perturbation. As shown in Figure 6b, the Device C shows longer charge recombination lifetime of 1.29 µs than 1.24 µs for the Device A and 1.09 µs for the Device B; however, the Device D with P-TPA shows a higher charge recombination lifetime of 1.85 µs than the Device C without P-TPA, suggesting that the charge recombination is low for the P-TPA processed device. To deeply investigate the origin of the improved J_{sc}, the space charge limited current (SCLC) characteristics of hole-only devices with ITO/CdTe(200 nm)/(w/o)P-TPA(20 nm)/Au configuration are measured (Figure 6c). The fitting curves are drawn based on the Mott–Gurney law[49]

$$J = \frac{9}{8}\varepsilon_0 \varepsilon_r \mu_p \frac{(V - V_{bi} - V_s)^2}{L^3} \tag{2}$$

where L is the thickness of the active layer and μ_p is the hole mobility of the CdTe NC thin film. It is evident that the μ_p is increased from 4.93×10^{-4} to 1.20×10^{-3} cm^2 V^{-1} s^{-1} with the insertion of P-TPA. The higher mobility for P-TPA processed device implies hole carrier transport is drastically enhanced in the help of crosslinkable polymer P-TPA HTL, and thus a very high J_{sc} is expected for the CdTe NC Device D with P-TPA. Based on the *C–V*, TPV and SCLC results, we speculate that a dipole layer is formed when the P-TPA layer is incorporated at the CdTe/Au interface.[50] As presented in Figure 6d, the formation of the dipole layer connecting the CdTe active layer and contact electrode causes a vacuum energy level shift and thus facilitates hole extraction due to the reduced hole injection barrier. Finally the electron/hole recombination at the CdTe/Au interface will be decreased and correspondingly a high output photocurrent is expected.

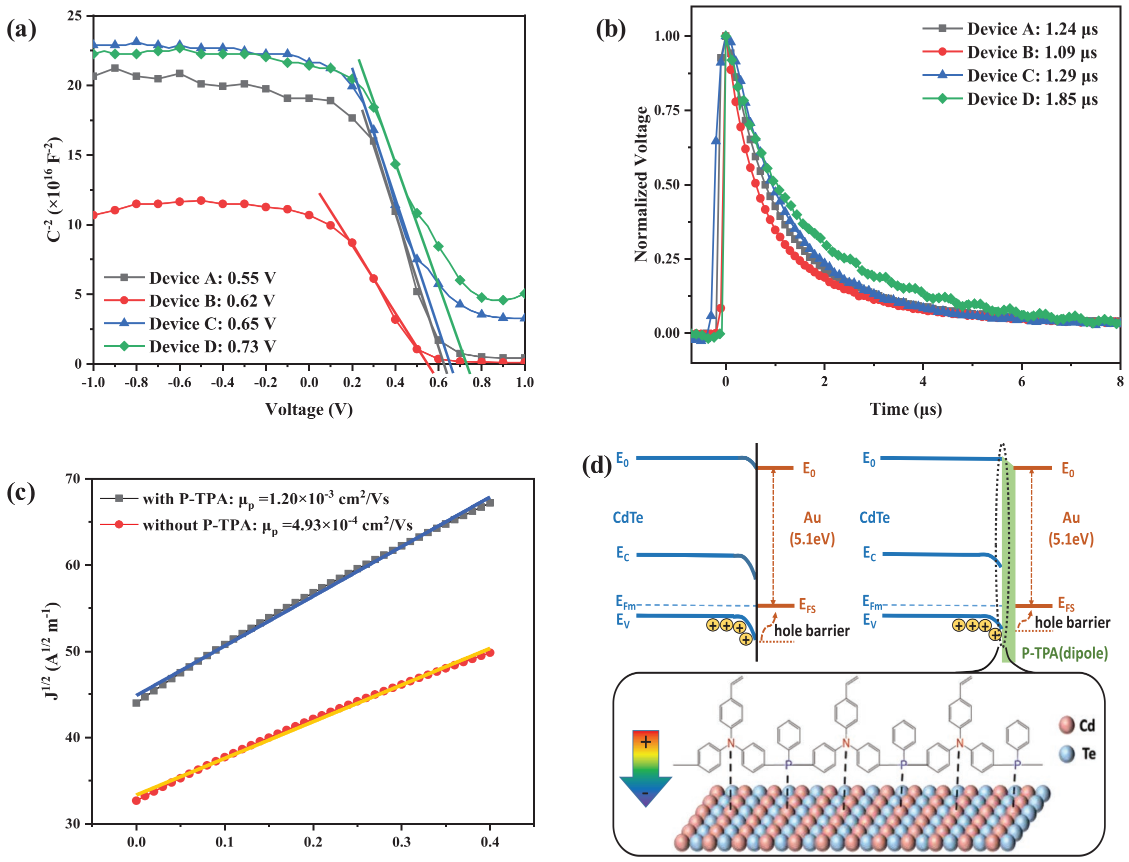

Figure 6. a) Mott–Schottky *C–V* curve and b) transient photovoltage (TPV) measurements of four kinds of CdTe NC solar cells; c) SCLC measurements of hole-only devices (device structure: ITO/CdTe(200 nm)/P-TPA(w/o)/Au; d) A schematic of energy levels influenced by a dipole layer of P-TPA at the CdTe/Au interface.

3. Conclusion

In summary, we have demonstrated a novel strategy of interface engineering for both cathode and anode to enable high-efficiency solution-processed CdTe nanocrystal solar cells. By incorporating CdS/CdSe gradient ETLs, simultaneous enhancements of J_{sc} and V_{oc} are obtained, which is mainly attributed to the reduced carrier recombination and electron injection barrier at the cathode interfaces. Moreover, by inserting a thin layer of crosslinkable P-TPA at the CdTe/Au interface, higher V_{bi} and hole mobility as well as carrier lifetime are obtained, which is essential for efficient hole carrier extraction. In the end, the PCE of the device with interface engineering of both cathode and anode is improved to 9.2%, which is the highest value ever reported among solution-processed CdTe NC solar cells with a superstrate structure. This work illustrates a new route for further improving solution-processed CdTe NC device performance by optimizing the cathode/anode interfaces with hybrid inorganic/organic thin films.

4. Experimental Section

Device Fabrication: CdS NC, CdSe NC, CdTe NC, and ZnO precursor were synthesized based on literature-reported methods.[51–54] P-TPA was purchased from Canton OLEDKING Optoelectric Materials Co. Ltd and used as received. ZnO precursor was spin-coated onto the ITO at a speed of 3000 rpm for 20 s under ambient conditions. Then the sample was annealed at 200 °C for 10 min to convert into the ZnO thin film and at 400 °C for 10 min to eliminate any organic impurities. CdS, CdSe, and CdTe NC films were deposited in sequence using a layer-by-layer spin-coating solution process under ambient conditions. The detailed fabrication process can be found in the previous literature.[51,52] To prepare the P-TPA HTL, P-TPA was dissolved in o-xylene with a concentration of 6 mg mL^{-1}. Several drops of P-TPA solution was dropped onto the CdTe NC thin film and spun at 2000 rpm for 20 s. The substrate was then annealed at 120 °C for 10 min to thermally crosslink P-TPA and eliminate any solvent. Finally, a gold electrode (80 nm) was deposited via thermal evaporation through a shadow mask with an active area of 0.16 cm^2.

Characterization: The electrochemical cyclic voltammetry was conducted on a CHI660E Electrochemical Workstation, in a 0.1 mol L^{-1} acetonitrile solution of tetrabutylammonium hexafluorophosphate (n-Bu$_4$NPF$_6$) at a potential scan rate of 0.1 V s^{-1} with an Ag/AgCl reference electrode and a platinum wire counter electrode. Polymer film was formed by drop-casting P-TPA solution in chloroform (1 mg mL^{-1}) onto the working electrode, and then dried in the air. UV–vis absorption spectrum were obtained using a Shimadzu 3600 UV–vis–NIR spectrophotometer. The focused ion beam cross sections across ITO/ZnO/CdS/CdSe/CdTe/P-TPA/Au devices were obtained using a FEI Helios 450S dual beam FIB. The TEM images and EDS images were recorded with a FEI Titan Themis 200 TEM that was fitted with the bright-field, high-angle annular dark-field, and EDS

(Bruker super-X EDS, Bruker). The samples were sputtered with a thin layer of carbon before recording. The SCLC measurement and current density–voltage characterization under dark and 100 mW cm^{-2} (AM 1.5G) illumination from solar simulator (XES-40S1, SAN-EI electric) were carried out on computer-controlled Keithley 2400 Source Meter measurement system in air. EQE measurements were recorded utilizing a spectral response/quantum efficiency measurement testing system (QE-R3011, Enlitech). The *C–V* measurements were recorded from an impedance analyzer (HP-4192A, Hewlett Packard) in the dark at 1000 Hz from −1.0 to 1.0 V. TPV measurements were taken by using the OmniFluo system (Zolix Co.). The work function of CdTe was estimated by photoelectron spectroscopy in air (PESA, AC-3, Rikken Keiki Co.) in 4.0–7.0 eV energy search range with step 0.1 eV.

Supporting Information

Supporting Information is available from the Wiley Online Library or from the author.

Acknowledgements

The authors thank the financial support of the National Natural Science Foundation of China (Nos. 21875075, 61774077, 61274062, and 21174042), Guangdong Province Natural Science Fund (Nos. 2018A0303130041), Guangzhou Science and Technology Plan Project (201804010295).

Conflict of Interest

The authors declare no conflict of interest.

Keywords

CdTe, interface engineering, nanocrystal, solar cells, solution processed

Received: May 17, 2019
Revised: July 17, 2019

[1] J. M. Kurley, M. G. Panthani, R. W. Crisp, S. U. Nanayakkara, G. F. Pach, M. O. Reese, M. H. Hudson, D. S. Dolzhnikov, V. Tanygin, J. M. Luther, D. V. Talapin, *ACS Energy Lett.* **2017**, *2*, 270.
[2] M. Yuan, M. Liu, E. H. Sargent, *Nat. Energy* **2016**, *1*, 16016.
[3] T. Kim, Y. Firdaus, A. R. Kirmani, R. Z. Liang, H. Hu, M. Liu, A. E. Labban, S. Hoogland, P. M. Beaujuge, E. H. Sargent, A. Amassian, *ACS Energy Lett.* **2018**, *3*, 1307.
[4] J. Kim, O. Ouellette, O. Voznyy, M. Wei, J. Choi, M. Choi, J. WoongJo, S. Baek, J. Fan, M. I. Saidaminov, B. Sun, P. Li, D. Nam, S. Hoogland, Z. Lu, F. Pelayo García de Arquer, E. H. Sargent, *Adv. Mater.* **2018**, *30*, 1803830.
[5] Z. Yang, J. Z. Fan, A. H. Proppe, F. Pelayo García de Arquer, D. Rossouw, O. Voznyy, X. Lan, M. Liu, G. Walters, R. Quitero-Bermudez, B. Sun, S. Hoogland, G. A. Botton, S. O. Kelly, E. H. Sargent, *Nat. Commun.* **2017**, *8*, 1325.
[6] H. Xue, R. Wu, Y. Xie, Q. Tan, D. Qin, H. Wu, W. Huang, *Appl. Sci.* **2016**, *6*, 197.
[7] G. Jin, N. Chen, Q. Zeng, F. Liu, W. Yuan, S. Xiang, T. Feng, X. Hu, T. Ji, L. Wang, Y. Wang, H. Sun, H. Sun, B. Yang, *Adv. Energy Mater.* **2018**, *8*, 1701966.
[8] I. Gur, N. A. Fromer, M. L. Geier, A. P. Alivisatos, *Science* **2005**, *310*, 462.
[9] M. G. Panthani, J. M. Kurley, R. W. Crisp, T. C. Dietz, T. Ezzyat, J. M. Luther, D. V. Talapin, *Nano Lett.* **2014**, *14*, 670.
[10] B. I. MacDonald, A. Martucci, S. RuBano, S. Watkins, P. Mulvaney, J. J. Jasieniak, *ACS Nano* **2012**, *6*, 5995.
[11] J. Jasieniak, B. I. Macdonald, S. E. Watkins, P. Mulvaney, *Nano Lett.* **2011**, *11*, 2856.
[12] Q. Zeng, L. Hu, J. Cui, T. Feng, X. Du, G. Jin, F. Liu, T. Ji, F. Li, H. Zhang, B. Yang, *ACS Appl. Mater. Interfaces* **2017**, *9*, 31345.
[13] Z. Chen, H. Zhang, Q. Zeng, Y. Wang, D. Xu, L. Wang, H. Wang, B. Yang, *Adv. Energy Mater.* **2014**, *4*, 1400235.
[14] W. Yoon, T. K. Townsend, M. P. Lumb, T. G. Tischler, E. E. Foos, *IEEE Trans. Nanotechnol.* **2014**, *13*, 551.
[15] R. W. Crisp, G. F. Pach, J. M. Kurley, R. M. France, M. O. Reese, S. U. Nanayakkara, B. A. MacLeod, D. V. Talapin, M. C. Beard, J. M. Luther, *Nano Lett.* **2017**, *17*, 1020.
[16] X. Du, Z. Chen, F. Liu, Q. Zeng, G. Jin, F. Li, D. Yao, B. Yang, *ACS Appl. Mater. Interfaces* **2016**, *8*, 900.
[17] T. Yang, W. Cai, D. Qin, E. Wang, L. Lan, X. Gong, J. Peng, Y. Cao, *J. Phys. Chem. C* **2010**, *114*, 6849.
[18] R. W. Crisp, M. G. Panthani, W. L. Rance, J. N. Duenow, P. A. Parilla, R. Callahan, M. S. Dabney, J. J. Berry, D. V. Talapin, J. M. Luther, *ACS Nano* **2014**, *8*, 9063.
[19] Y. Tian, Y. Zhang, Y. Lin, K. Gao, Y. Zhang, K. Liu, Q. Yang, X. Zhou, D. Qin, H. Wu, Y. Xia, L. Hou, L. Lan, J. Chen, D. Wang, R. Yao, *J. Nanopart. Res.* **2013**, *15*, 1.
[20] M. Li, X. Liu, S. Wen, S. Liu, J. Heng, D. Qin, L. Hou, H. Wu, W. Xu, W. Huang, *Nanomaterials* **2017**, *7*, 101.
[21] J. M. Burst, J. N. Duenow, D. S. Albin, E. Colegrove, M. O. Reese, J. A. Aguiar, C. -S. Jiang, M. K. Patel, M. M. Al-Jassim, D. Kuciauskas, S. Swain, T. Ablekim, K. G. Lynn, W. K. Metzger, *Nat. Energy* **2016**, *1*, 16015.
[22] L. Kranz, C. Gretener, J. Perrenoud, D. Jaeger, S. S. A. Gerstl, R. Schmitt, S. Buecheler, A. N. Tiwari, *Adv. Energy Mater.* **2014**, *4*, 1301400.
[23] S. G. Kumar, K. S. R. K. Rao, *Energy Environ. Sci.* **2014**, *7*, 659.
[24] N. W. Duffy, L. M. Peter, R. L. Wang, *J. Electroanal. Chem.* **2002**, *532*, 207.
[25] L. A. Kosyachenko, E. V. Grushko, X. Mathew, *Sol. Energy Mater. Sol. Cells* **2012**, *96*, 231.
[26] K. Nakamura, M. Gotoh, T. Fujihara, T. Toyama, H. Okamoto, *Sol. Energy Mater. Sol. Cells* **2003**, *75*, 185.
[27] J. Perrenoud, L. Kranz, S. Buecheler, F. Pianezzi, A. N. Tiwari, *Thin Solid Films* **2011**, *519*, 7444.
[28] D. E. Swanson, J. R. Sites, W. S. Sampath, *Sol. Energy Mater. Sol. Cells* **2017**, *159*, 389.
[29] T. Baines, G. Zoppi, L. Bowen, T. P. Shalvey, S. Mariotti, K. Durose, J. D. Major, *Sol. Energy Mater. Sol. Cells* **2018**, *180*, 196.
[30] N. R. Paudel, Y. Yan, *Appl. Phys. Lett.* **2014**, *105*, 183510.
[31] P. J. Sebastian, *Thin Solid Films* **1994**, *245*, 132.
[32] J. P. Mangalhara, R. Thangaraj, O. P. Agnihotri, *Sol. Energy Mater.* **1989**, *19*, 157.
[33] N. R. Paudel, J. D. Poplawsky, K. L. Moore, Y. Yan, *IEEE J. Photovoltaics* **2015**, *5*, 1492.
[34] L. Kranz, C. Gretener, J. Perrenoud, R. Schmitt, F. Pianezzi, F. L. Mattina, P. Blosch, E. Cheah, A. Chirila, C. M. Fella, H. Hagendorfer, T. Jager, S. Nishiwaki, A. R. Uhl, S. Buecheler, A. N. Tiwari, *Nat. Commun.* **2013**, *4*, 2306.
[35] J. H. Yun, K. H. Kim, D. Y. Lee, B. T. Ahn, *Sol. Energy Mater. Sol. Cells* **2003**, *75*, 203.
[36] S. H. Demtsu, D. S. Albin, J. R. Sites, W. K. Metzger, A. Duba, *Thin Solid Films* **2008**, *516*, 2251.

[37] X. Guo, Q. Tan, S. Liu, D. Qin, Y. Mo, L. Hou, A. Liu, H. Wu, Y. Ma, *Nano Energy* **2018**, *46*, 150.
[38] D. B. Holt, *J. Phys. Chem. Solids* **1966**, *27*, 1053.
[39] K. Durose, D. Boyle, A. Abken, C. J. Ottley, P. Nollet, S. Degrave, M. Burgelman, R. Wendt, J. Beier, D. Bonnet, *Phys. Status Solidi B* **2002**, *229*, 1055.
[40] K. Wang, P. Jiang, Z. Zhang, Q. Fu, Y. Li, *Macromol. Chem. Phys.* **2013**, *214*, 1772.
[41] M. Jamal, M. S. Abu-Jafar, A. H. Reshak, *J. Alloys Compd.* **2016**, *667*, 151.
[42] M. Lingg, A. Spescha, S. G. Haass, R. Carron, S. Buecheler, A. N. Tiwari, *Sci. Technol. Adv. Mater.* **2018**, *19*, 683.
[43] J. Liu, W. Yang, Y. Li, L. Fan, Y. Li, *Phys. Chem. Chem. Phys.* **2014**, *16*, 4778.
[44] S. H. Wei, S. B. Zhang, A. Zunger, *J. Appl. Phys.* **2000**, *87*, 130.
[45] N. R. Paudel, A. D. Compaan, Y. Yan, *J. Electron. Mater.* **2014**, *43*, 2783.
[46] M. Yuan, D. Zhitomirsky, V. Adinolfi, O. Voznyy, K. W. Kemp, Z. Ning, X. Lan, J. Xu, J. Y. Kim, H. Dong, E. H. Sargent, *Adv. Mater.* **2013**, *25*, 5586.
[47] G. R. Perumallapelli, S. R. Vasa, J. Jang, *Org. Electron.* **2016**, *31*, 142.
[48] J. Zhu, Y. Yang, Y. Gao, D. Qin, H. Wu, L. Hou, W. Huang, *Nanotechnology* **2014**, *25*, 365203.
[49] R. Ciach, Y. P. Dotsenko, V. V. Naumov, A. N. Shmyryeva, P. S. Smertenko, *Sol. Energy Mater. Sol. Cells* **2003**, *76*, 613.
[50] M. Timpel, M. V. Nardi, G. Ligorio, B. Wegner, M. Pätzel, B. Kobin, S. Hecht, N. Koch, *ACS Appl. Mater. Interfaces* **2015**, *7*, 11900.
[51] S. Liu, W. Liu, J. Heng, W. Zhou, Y. Chen, S. Wen, D. Qin, L. Hou, D. Wang, H. Xu, *Coatings* **2018**, *8*, 26.
[52] H. Liu, Y. Tian, Y. Zhang, K. Gao, K. Lu, R. Wu, D. Qin, H. Wu, Z. Peng, L. Hou, W. Huang, *J. Mater. Chem. C* **2015**, *3*, 4227.
[53] S. Wen, M. Li, J. Yang, X. Mei, B. Wu, X. Liu, J. Heng, D. Qin, L. Hou, W. Xu, D. Wang, *Nanomaterials* **2017**, *7*, 380.
[54] Y. Xie, Q. Tan, Z. Zhang, K. Lu, M. Li, W. Xu, D. Qin, Y. Zhang, L. Hou, H. Wu, *J. Mater. Chem. C* **2016**, *4*, 6483.